


# Contents

<b>1</b>	<b>Introduction</b>	<b>4</b>
1.1	Magnetic Fields through the Zeeman Effect . . . . .	6
1.2	Magnetic Fields through Polarimetry . . . . .	7
<b>2</b>	<b>Research Methods</b>	<b>9</b>
2.1	Radio Interferometry . . . . .	10
2.2	Data Reduction with <i>Miriad</i> . . . . .	15
2.3	Code Repositories . . . . .	20
	<b>3</b> <del>Journal Paper</del> write the title of the paper	<b>21</b>
<b>4</b>	<b>Conclusion</b>	<b>32</b>
<b>5</b>	<b>Acknowledgments</b>	<b>32</b>
<b>6</b>	<b>References</b>	<b>33</b>

$\rightarrow$  polarized perpendicular to  $B_{POS}$ , ~~where the amount by which they are polarized is determined by the strength of the magnetic field.~~ In principle by measuring the size of the split and the full polarization state of the three components one can obtain full information about  $\vec{B}$  (Crutcher, 2012). However, except for ~~X~~ OH masers in a few cases, the Zeeman split is usually smaller than the linewidth of the spectral line, which limits the amount of information that can be obtained to  $B_{LOS}$  (Crutcher, 2012). In addition, for molecules with small  $Z$  factors, no net circular polarization is expected from the Zeeman effect since the  $\sigma$ -components, which are equal in strength and opposite in polarization, overlap (Crutcher, 2012). For this reason the discovery of circular polarization in the molecule CO was surprising and required a different mechanism to explain <sup>it,</sup> in view of its extremely low sensitivity to the Zeeman effect (Houde et al., 2013; Houde, 2014).

## 1.2 Magnetic Fields through Polarimetry

Maps of the magnetic field like that shown in Figure 1 are made by measuring the polarization state of the light incident on a telescope. At millimetre and submillimetre wavelengths, inferring the magnetic field from the measured polarization state is usually done either through broadband measurements of continuum thermal dust emission or using rotational transitions of molecules, like CO. Measuring molecular transitions has the advantage of brighter intensities compared to measuring thermal dust emission. In addition, by selecting different molecules we can obtain information on gas dynamics and detail about the structure of the cloud. This section will give a brief overview of the two methods and will give context to certain challenges with polarimetry of molecular spectral lines that the work presented here highlights.

The mechanisms that give rise to polarized light from dust versus from molecules are, though different, both related to the presence of a magnetic field in the local environment. It is generally expected that dust grains align themselves with their long

axis perpendicular to the magnetic field due to asymmetric radiative torques, causing any thermal emission from long grains to be linearly polarized perpendicular to the field (Andersson et al., 2015). Molecules will also preferentially align to the magnetic field because of the magnetic moment associated with their rotational transitions. In addition, a molecule in a magnetic field in a medium subjected to some anisotropy (e.g., in the ambient radiation field or the optical depth) will exhibit a net linear polarization level due to the resulting imbalance in the populations of the levels leading to the  $\pi$ - and  $\sigma$ -lines (Goldreich & Kylafis, 1981; Crutcher, 2012). This is referred to as the Goldreich-Kylafis (GK) effect and results in molecules emitting a small percentage of radiation that is linearly polarized either perpendicular or parallel to the plane of the sky component of the magnetic field  $B_{POS}$  (Goldreich & Kylafis, 1981). The degeneracy in the direction of the magnetic field is usually resolved by measuring continuum emission along with molecular emission, or by measuring several molecular transitions (Crutcher, 2012).

If we imagine molecules in a cloud subject to the effects of both a local magnetic field and turbulent motion, then we would expect that the stronger the magnetic field is relative to the turbulence in that region ~~the better the alignment is of dust and molecules with the field~~, since turbulence would have the effect of disturbing this alignment. Therefore if we observe a large dispersion in ~~polarization angles (PAs)~~ <sup>PA</sup> ~~angles (PAs)~~ <sup>PA</sup>

in a region then we might conclude that the field there is weaker than in a region where the PAs are more uniform, assuming the same level of turbulence. This idea is formally expressed by the Davis-Chandrasekhar-Fermi (DCF) method where the measured dispersion of PAs and particle velocities can be used to calculate ~~a value~~ <sup>the strength</sup>

~~for~~ the plane of the sky component of the magnetic field according to

$$B_{POS} = \sqrt{4\pi\rho} \frac{\delta V}{\delta\phi}, \quad (5)$$

where  $\rho$  is the gas mass density,  $\delta V$  is the velocity dispersion of the particles in the cloud (and is a measure of the level of turbulence) and  $\delta\phi$  is the dispersion in PAs (Davis, 1951; Chandrasekhar & Fermi, 1953; Crutcher, 2012). This method has proven useful in estimating the magnetic field in molecular clouds and in the galactic plane (Chandrasekhar & Fermi, 1953; Crutcher, 2012), and has seen several extensions and refinements in recent years (Houde, 2004; Hildebrand et al., 2009; Houde et al., 2009).

Since the PA is the critical piece of information that connects polarization measurements to the orientation of the magnetic field, any effects that ~~rotate~~<sup>change</sup> the PA will taint the measurement of the magnetic field. Two important examples of this that concern this report are the presence of polarized light due to the telescope’s instrumentation (e.g.: Hamaker et al., 1996; Sault et al., 1996; Marrone et al., 2008) and anisotropic resonant scattering (ARS) from molecular transitions, which can convert linear polarization (LP) to circular polarization (CP) along the line of sight (Houde et al., 2013; Hezareh et al., 2013; Houde, 2014). Since it may be possible to retrieve the ‘lost’ LP by measuring CP (Hezareh et al., 2013), and the ARS effect may be a common occurrence in molecular clouds (this work), measuring CP simultaneously with LP when doing molecular spectral line polarimetry may be essential to obtaining accurate measurements of the magnetic field.

## 2 Research Methods

The data presented in the attached paper were collected from the archive of the Submillimeter Array (SMA), an array of eight 6m radio telescopes located at Mauna Kea, Hawaii. This section will describe the basic principles of radio interferometry, how polarimetric data is collected with the SMA, and an overview of the data reduction process using the *Miriad* data reduction package (Sault et al., 1995).

## 2.1 Radio Interferometry

Radio interferometry is a technique for obtaining high-resolution maps of objects in the sky that avoids building gigantic primary reflectors and relies on computationally intensive data analysis tasks.

Since the angular resolution of a telescope goes as  $\theta \propto \lambda/D$ , where  $\lambda$  is the wavelength and  $D$  is the diameter of the primary reflector, we try to build larger and larger mirrors and dishes to obtain higher resolution. However, reflectors that are large enough become very challenging to build when seeking resolutions of  $< 1''$  at radio wavelengths. To illustrate how we can attain a higher resolution without building a massive reflector, consider a dish with a diameter 500 m across: this dish gives us high resolution but is beyond our ability to manufacture. Imagine now that we remove or obstruct large sections of this reflector. The images we would obtain from such a “patchy” reflector are now in fact the Fourier transform of the intensity map of the object being examined on the sky, much like how the support struts on, for example, Hubble, cause imaged stars to appear to have a superimposed cross pattern. With radio interferometry, we obtain the resolution of a large dish by sampling the light it would receive and inferring the true sky image by inverting the measured Fourier transform.

The resolution of the interferometer array is determined by the longest baseline separation  $B_{max}$  between any two elements of the array. This  $B_{max}$  is effectively the diameter of our “patchy” reflector. However, while the resolution defines the scale of the smallest object that is resolvable, an interferometer also has a limit on the largest resolvable scale, which is defined by the shortest baseline  $B_{min}$  of any two elements in the array. This implies that large spatial emission will be filtered out by the interferometer.

The output of a radio interferometer is the visibility function  $\mathcal{V}(u, v)$ , which is found by correlating the voltage signals from ~~a~~<sup>all</sup> pair<sup>s</sup> of antennae. This correlation is

done on-the-fly by an onsite computer, the so-called correlator, and the raw voltage signals are often discarded after the correlation is computed due to the prohibitively large amount of data. The arguments  $u$  and  $v$  are related to the distances between the two antennae. Given antennae  $a$  and  $b$  the visibility is written as

$$\mathcal{V}(u, v) = \frac{\langle V_a(t) \star V_b(t) \rangle}{A_0 \Delta \nu}, \quad (6)$$

where  $V_a(t)$  and  $V_b(t)$  are the measured voltage signals from antennae  $a$  and  $b$ ,  $A_0$  is the collecting area of the dish,  $\Delta \nu$  is the bandwidth of the receiver, and  $\langle V_a(t) \star V_b(t) \rangle$  denotes the time-averaged cross-correlation of the voltage signals, which is defined by

$$\langle V_a(t) \star V_b(t) \rangle = \lim_{T \rightarrow \infty} \frac{1}{2T} \int_{-T}^T V_a(t) V_b^*(t - \tau) dt. \quad (7)$$

Here  $\tau$  is a delay parameter that is chosen based on the type of observations being made (Thompson et al., 2001).

The expression shown in eq. (6) can be shown to be equivalent to the Fourier transform of the intensity map (the image)  $I(l, m)$ , where  $l$  and  $m$  are angular positions, through the van Cittert-Zernicke theorem. In its most general form the van Cittert-Zernicke theorem proves that incoherent radiation observed from a large distance appears to be coherent (see Chap. 14 of Thompson et al., 2001, for a derivation). Here we prove a consequence of it as it relates to interferometry to show that  $\mathcal{V}(u, v) = \mathcal{F}\{I(l, m)\}$ , where  $\mathcal{F}\{\}$  denotes the Fourier transform.

Consider two antennae  $a$  and  $b$  at positions  $(x_a, y_a)$  and  $(x_b, y_b)$ , pointed at the same object. The electric field at antennae  $a$  and  $b$  from sky position  $(l, m)$  at time  $t$  is given by

$$E_a(l, m, t) = A(l, m, t) e^{i\phi(l, m, t) + 2\pi i(x_a l + y_a m)} \quad (8)$$

$$E_b(l, m, t) = A(l, m, t) e^{i\phi(l, m, t) + 2\pi i(x_b l + y_b m)}, \quad (9)$$

are you missing a "t" in the denominator?

where  $A(l, m, t)$  is the amplitude of the field and  $\phi(l, m, t)$  is the phase of the wave which van Cittert-Zernicke tells us is the same in both  $E_a(l, m, t)$  and  $E_b(l, m, t)$  since the waves appear as coherent. The total voltage response of the antenna's receiver is the superposition of all electromagnetic waves from each position of the object, which can be written as:

$$V_a(t) = \int_{l,m} E_a(l, m, t) dl dm = \int_{l,m} \int_{\nu} E_a(l, m, \nu) e^{2\pi i \nu t} d\nu dl dm \quad (10)$$

$$V_b(t) = \int_{l,m} E_b(l, m, t) dl dm = \int_{l,m} \int_{\nu} E_b(l, m, \nu) e^{2\pi i \nu t} d\nu dl dm, \quad (11)$$

where we chose to express  $E(l, m, t)$  in terms of its Fourier transform. We will also write  $E(l, m, \nu) = A(l, m, \nu) e^{i\phi(l, m, \nu)} e^{2\pi i(xl + ym)}$ . The complex product is now

$$\begin{aligned} V_a(t) V_b^*(\lambda) &= \int_{l,m} \int_{\nu} E_a(l, m, \nu) e^{2\pi i \nu t} d\nu dl dm \times \int_{l',m'} \int_{\nu'} E_b^*(l', m', \nu') e^{-2\pi i \nu' \lambda} d\nu' dl' dm' \\ &= \int_{l,m} \int_{l',m'} \int_{\nu} \int_{\nu'} A(l, m, \nu) A^*(l', m', \nu') e^{i\phi(l, m, \nu) + 2\pi i(x_a l + y_a m)} \\ &\quad e^{-i\phi(l', m', \nu') - 2\pi i(x_b l' + y_b m')} e^{2\pi i \nu t} e^{-2\pi i \nu' \lambda} d\nu d\nu' dl' dm' dl dm \\ &= \int_{l,m} \int_{l',m'} \int_{\nu} \int_{\nu'} A(l, m, \nu) A^*(l', m', \nu') e^{i\phi(l, m, \nu) - i\phi(l', m', \nu')} \\ &\quad e^{2\pi i(x_a l - x_b l' + y_a m - y_b m')} e^{2\pi i(\nu t - \nu' \lambda)} d\nu d\nu' dl' dm' dl dm \\ &= \int_{l,m} \int_{\nu} |A(l, m, \nu)|^2 e^{2\pi i \nu(t - \lambda)} e^{2\pi i(\Delta x l + \Delta y m)} d\nu dl dm, \end{aligned} \quad (12)$$

where the last line follows since

$$\int_{l,m} \int_{l',m'} \int_{\nu} \int_{\nu'} e^{i\phi(l, m, \nu)} e^{-i\phi(l', m', \nu')} d\nu d\nu' dl dm dl' dm' = \delta(\nu - \nu', l - l', m - m'), \quad (13)$$

and the other terms are constant relative to the  $e^{i\phi}$  terms. This is because even though both antennae measure the same phase  $\phi(l, m, \nu)$ , it varies extremely quickly across different spatial positions  $l$  and  $m$ . If we set  $\lambda = t - \tau$ , where  $\tau$  is the time lag

and frequency  $\nu$ .

I don't understand why you say that. I don't see how this could be... unless you are missing a 'd' in the denominator. Then  $u = 2\pi \frac{\Delta x}{\lambda}$ ?

$$V_a(t)V_b^*(t-\tau) = \int_{l,m} \int_{\nu} |A(l,m,\nu)|^2 e^{2\pi i \nu \tau} e^{2\pi i (\Delta x l + \Delta y m)} d\nu dl dm, \quad (14)$$

The positional arguments become  $u = \Delta x \equiv x_a - x_b$  and  $v = \Delta y \equiv y_a - y_b$ . Then, after time-averaging according to eq. (7) we finally obtain

$$\begin{aligned} \langle V_a(t)V_b^*(t-\tau) \rangle &= \lim_{T \rightarrow \infty} \frac{1}{2T} \int_{-T}^T \int_{l,m} \int_{\nu} |A(l,m,\nu)|^2 e^{2\pi i \nu \tau} e^{2\pi i (\Delta x l + \Delta y m)} d\nu dl dm dt \\ &= \int_{l,m} \int_{\nu} I(l,m,\nu) e^{2\pi i \nu \tau} e^{2\pi i (ul + vm)} d\nu dl dm \\ &= \mathcal{F}\{I(l,m,\nu)\}, \end{aligned} \quad (15)$$

where  $I(l,m) = |A(l,m)|^2$  (chap. 3 of Thompson et al., 2001; Vanderlinde, 2017).

Thus at a given frequency of observation  $\nu$  we can say that  $\langle V_a(t)V_b^*(t-\tau) \rangle_{\nu} = \mathcal{F}\{I(l,m,\nu)\}$ .

Equation (15) shows the Fourier transform connection between the cross-correlation and the intensity map  $I(l,m)$ . The intensity map is therefore obtained by performing an inverse 2D Fourier transform on the visibilities, which is of course limited by how well the visibilities have been measured. A single pair of antennae samples a single  $(u,v)$  point in visibility space, meaning that the more baselines there are in the array the better the  $uv$ -coverage and the more accurate the final map is. The  $uv$ -coverage is also greatly improved by the rotation of the Earth since different orientations relative to the object change the  $(u,v)$  coordinates (Thompson et al., 2001). Images formed from poorly sampled visibilities will result in a large number of periodic 'blobs' or 'stripes' on the image that are not real and are purely a side-effect of the periodic functions used to perform the Fourier transform.

To obtain maps at different frequencies the signal must be binned into different spectral channels before being correlated. To obtain maps of specific polarizations in

put '1-1' where needed